

**Tunneling conductance of normal metal / $d_{x^2-y^2}$ -wave
superconductor junctions in the presence of broken time reversal
symmetry states near interfaces**

Y. Tanuma*, Y. Tanaka

Department of Applied Physics, Nagoya University, Nagoya 464-8063, Japan

S. Kashiwaya

Electrotechnical Laboratory, 1-1-4 Umezono, Tsukuba, 305-0045, Japan

(October 30, 2018)

Abstract

In order to clarify the influence of (the presence of) the broken time-reversal symmetry state (BTRSS) induced near the interface, tunneling conductance spectra in normal metal / $d_{x^2-y^2}$ -wave superconductor junctions are calculated on the basis of the quasiclassical Green's function method. The spatial dependence of the pair potential in the superconductor side is determined self-consistently. We discuss two types of the symmetry on the BTRSS; i) $d_{x^2-y^2}+is$ -wave state and ii) $d_{x^2-y^2}+id_{xy}$ -wave state. It is shown that the amplitude of the subdominant component (is -wave or id_{xy} -wave) is quite sensitive to the transmission coefficient of the junction. As the results, the splitting of the zero-bias conductance peak due to the BTRSS inducement is detectable only at junctions with small transmission coefficients for both cases. When the transmission coefficients are relatively large, the explicit peak splitting does not occur and the difference in the two cases appears in the height of

the zero-bias peaks.

PACS numbers: 74.50.+r, 74.20.Rp, 74.72.-h

I. INTRODUCTION

Identifying of the pairing symmetry in high- T_c superconductors is important to clarify the mechanism of the superconductivity. A great deal of experimental and theoretical studies have revealed that the superconducting pair potential has $d_{x^2-y^2}$ -wave symmetry in the bulk state¹⁻⁴. Since the pair potential of the $d_{x^2-y^2}$ -wave superconductor is anisotropic, the amplitude of the pair potential near the surface or interface is significantly reduced. This suppression of the pair potential causes a very interesting phenomena, *i.e.* the formation of Andreev bound state (ABS) at the Fermi energy (zero-energy) near a specularly reflecting surface⁵ when the angle between the lobe direction of the $d_{x^2-y^2}$ -wave pair potential and the normal to the interface is nonzero. This state is originated from the interference effect in the effective pair potential of the $d_{x^2-y^2}$ -wave symmetry through the reflection at the surface or interface. The ABS manifests itself as a sharp peak in the middle of the tunneling conductance spectra, the so-called zero-bias conductance peak (ZBCP),⁶ and the consistency between theory and experiments has been checked in details^{4,7,9-15}.

On the other hand, there still remains a controversial issue; formation of a broken time reversal symmetry state (BTRSS) at low temperature due to the mixing of subdominant s -,¹⁶⁻¹⁸ or d_{xy} -wave component¹⁹⁻²¹ as the imaginary part of the pair potential to the predominant $d_{x^2-y^2}$ -wave component²⁵. Theoretical studies based on the quasiclassical approximation^{25,26} and several lattice models^{28,29} reported the presence of the induced subdominant pair potential near the surface which breaks the time reversal symmetry²⁵. The resulting surface density of states with the BTRSS shows the splitting of the zero-energy peak²⁵ and the corresponding tunneling conductance shows the ZBCP splitting. It has also been clarified that the magnitude of the splitting depends on the induced subdominant pair potential near the surface. Actually, Covington *et al.*²², Krupke *et al.*²³, and Sharoni *et al.*²⁴ reports the ZBCP splitting at low temperature and they ascribed the origin of the ZBCP splitting to the above BTRSS³⁰. However, at the same time, there are many experiments which do not show the ZBCP splitting, and in these experiments, ZBCP survives even at

low temperatures^{4,12,14,15,13}. Although there are several pre-existing theories which discuss the BTRSS²⁵, almost all these theories treat the semi-infinite $d_{x^2-y^2}$ -wave superconductor and the relevance to the actual experiments of tunneling spectroscopy has not been fully clarified yet. At this stage, it is an important problem to clarify the stability and the possible observability of the formation of BTRSS, *i.e.*, the ZBCP splitting, for various condition of the junctions. There are several factors which determine the magnitude of the splitting of ZBCP; (i) inter-electron potential which induces the subdominant pair potential near the interface, (ii) transmission probability of the particles at the interface, (iii) orientation of the junctions, *i.e.*, the angle between the normal to the interface and the crystal axis of $d_{x^2-y^2}$ -wave superconductor, (iv) finite temperature effect, (v) roughness of the interface²⁷, and (vi) impurity concentration in the superconductor³¹.

Although there are several factors which determine the magnitude of the splitting of ZBCP, in this paper, we concentrate on (i), (ii), (iii), and (iv). First, we calculate the spatial variation of the pair potential in the normal metal / $d_{x^2-y^2}$ -wave superconductor junction (N/D junction) in the presence of subdominant pair potential using a quasiclassical formalism for various conditions of the junctions. Using these results, we calculate tunneling conductance.

The organization of this paper is as follows. In Sec. II, a formulation to calculate the spatial dependence of the pair potential, and the tunneling conductance is presented. In Sec. III, results of the numerical calculations for both $d_{x^2-y^2}+is$ - and $d_{x^2-y^2}+id_{xy}$ -wave states are discussed in detail. Section IV is devoted to conclusions and future problems.

II. THEORETICAL FORMULATION

We study N/D junctions in the clean limit, where the normal metal is located at $x < 0$ and the $d_{x^2-y^2}$ -wave superconductor extends elsewhere. For the simplicity, two dimensional system is assumed and the x -axis is taken perpendicular to the flat interface located at $x = 0$. When quasiparticles are in the xy -plane, a transmitted electron-like quasiparticle and hole-

like quasiparticle feel different effective pair potentials $\Delta(\phi_+)$ and $\Delta(\phi_-)$, with $\phi_+ = \phi$ and $\phi_- = \pi - \phi$. Here, ϕ is the azimuthal angle in the xy -plane given by $(k_x + ik_y)/|\mathbf{k}| = e^{i\phi}$. The barrier potential at the interface has a δ -functional form $H\delta(x)$, where $\delta(x)$ and H are the δ -function and its amplitude, respectively. A cylindrical Fermi surface is assumed and the magnitude of the Fermi momentum and the effective mass are chosen to be equal both in the normal metal and in the superconductor.

The quasiclassical Green's function method^{25,26,32–38} developed by Ashida *et al.*^{39,40} is used in order to determine the spatial variation of the pair potential self-consistently. In the following, we briefly summarize this quasiclassical method we used. We start with the Bogoliubov-de Gennes (BdG) equation for unconventional spin-singlet superconductors^{33,41},

$$E_n \tilde{u}_n(\mathbf{r}) = H_0 \tilde{u}_n(\mathbf{r}) + \int d\mathbf{r}' \Delta(\mathbf{r}, \mathbf{r}') \tilde{v}_n(\mathbf{r}'), \quad (1)$$

$$E_n \tilde{v}_n(\mathbf{r}) = -H_0 \tilde{v}_n(\mathbf{r}) + \int d\mathbf{r}' \Delta^*(\mathbf{r}, \mathbf{r}') \tilde{u}_n(\mathbf{r}'), \quad (2)$$

$$H_0 = -\frac{\hbar^2}{2m} \nabla^2 - \mu, \quad (3)$$

where μ is the chemical potential, while $\tilde{u}_n(\mathbf{r})$ and $\tilde{v}_n(\mathbf{r})$ denote the electron-like and hole-like components of the wave function,

$$\begin{aligned} \tilde{\Psi}_n(\mathbf{r}) &= \begin{pmatrix} \tilde{u}_n(\mathbf{r}) \\ \tilde{v}_n(\mathbf{r}) \end{pmatrix}, \\ &\equiv \begin{pmatrix} u_n(\hat{\mathbf{k}}, \mathbf{r}) \\ v_n(\hat{\mathbf{k}}, \mathbf{r}) \end{pmatrix} e^{ik_F \cdot \mathbf{r}} = \Psi_n(\hat{\mathbf{k}}, \mathbf{r}) e^{ik_F \cdot \mathbf{r}}. \end{aligned} \quad (4)$$

Here the quantities $\hat{\mathbf{k}}$ and \mathbf{r} stand for the unit vector of the wave number of the Cooper pair which is fixed on the Fermi surface ($\hat{\mathbf{k}} = \mathbf{k}_F/|\mathbf{k}_F|$), and the position of the center of mass of Cooper pair, respectively. After applying the quasiclassical approximation, the BdG equation is reduced to the Andreev equation^{5,33,42},

$$E_n \Psi_n(\hat{\mathbf{k}}, \mathbf{r}) = - \left[i\hbar v_F \hat{\mathbf{k}} \cdot \nabla + \hat{\Delta}(\hat{\mathbf{k}}, \mathbf{r}) \right] \hat{\tau}_3 \Psi_n(\hat{\mathbf{k}}, \mathbf{r}), \quad (5)$$

$$\hat{\Delta}(\hat{\mathbf{k}}, \mathbf{r}) = \begin{pmatrix} 0 & \Delta(\hat{\mathbf{k}}, \mathbf{r}) \\ -\Delta^*(\hat{\mathbf{k}}, \mathbf{r}) & 0 \end{pmatrix}, \quad (6)$$

where v_F and $\hat{\tau}_i (i = 1, 2, 3)$ stand for Fermi velocity and Pauli matrices, respectively. The wave function $\Psi_n(\hat{\mathbf{k}}, \mathbf{r})$ is obtained by neglecting the rapidly oscillating plane-wave part following the quasiclassical approximation^{33,42}. The $\hat{\mathbf{k}}$ dependence of $\Delta(\hat{\mathbf{k}}, \mathbf{r})$ represents the symmetry of the pair potential.

Now, we consider the case where a specularly reflecting surface or interface runs along the y -direction. In this case, the pair potential depends only on x since the system is homogeneous along the y -direction. It is convenient to introduce the following directional notation,^{25,39}

$$\begin{aligned} \Psi_n(\hat{\mathbf{k}}, \mathbf{r}) &= \Phi_n^{(+)}(\phi_+, x)e^{i|k_{Fx}|x} + \Phi_n^{(-)}(\phi_-, x)e^{-i|k_{Fx}|x}, \\ \Phi_n^{(\alpha)}(\phi_\alpha, x) &= \begin{pmatrix} u_n^{(\alpha)}(\phi_\alpha, x) \\ v_n^{(\alpha)}(\phi_\alpha, x) \end{pmatrix}. \end{aligned} \quad (7)$$

Here \pm represents the sign of the x component of the Fermi wave number k_{Fx} and $\alpha(\beta) = \pm$. We define a Green's function $G_{\alpha\beta}(\phi, x, x')$ and a quasiclassical Green's function $g_{\alpha\beta}(\phi, x)$,

$$G_{\alpha\beta}(\phi, x, x') = \sum_n \frac{\Phi_n^{(\alpha)}(\phi_\alpha, x)\Phi_n^{(\beta)\dagger}(\phi_\beta, x)}{i\omega_m - E_n}, \quad (8)$$

$$g_{\alpha\beta}(\phi, x) \pm i(\hat{\gamma}_3)_{\alpha\beta} = -2\hbar|v_{Fx}|\hat{\tau}_3 G_{\alpha\beta}(\phi, x \pm 0, x). \quad (9)$$

In the above, $\hat{\gamma}_3$ is the Pauli matrix in the directional space³⁹ and v_{Fx} is the x -component of the Fermi velocity. The quasiclassical Green's function $g_{\alpha\beta}(\phi, x)$ obeys the Eilenberger equation,³²

$$\begin{aligned} i|v_{Fx}|\frac{\partial}{\partial x}g_{\alpha\beta}(\phi, x) &= -\alpha \left[i\omega_m \hat{\tau}_3 + \hat{\Delta}(\phi_\alpha, x) \right] g_{\alpha\beta}(\phi, x) \\ &+ \beta g_{\alpha\beta}(\phi, x) \left[i\omega_m \hat{\tau}_3 + \hat{\Delta}(\phi_\beta, x) \right], \end{aligned} \quad (10)$$

$$\hat{\Delta}(\phi_\alpha, x) = \begin{pmatrix} 0 & \Delta(\phi_\alpha, x) \\ -\Delta^*(\phi_\alpha, x) & 0 \end{pmatrix}, \quad (11)$$

where ω_m is the Matsubara frequency. The quasiclassical Green's function can be written by the following evolution operator $U_\alpha(\phi_\alpha, x, x')$ as

$$g_{\alpha\beta}(\phi, x) = U_\alpha(\phi_\alpha, x, x')g_{\alpha\beta}(\phi, x')U_\beta^{-1}(\phi_\beta, x, x'), \quad (12)$$

where $U_\alpha(\phi_\alpha, x, x')$ satisfies the Andreev equation

$$i\hbar|v_{Fx}| \frac{\partial}{\partial x} U_\alpha(\phi_\alpha, x, x') = -\alpha \left[i\omega_m \hat{\tau}_3 + \hat{\Delta}(\phi_\alpha, x) \right] U_\alpha(\phi_\alpha, x, x'), \quad (13)$$

with $U_\alpha(\phi_\alpha, x, x) = 1$.

Considering a semi-infinite N/D junction geometry, the pair potential in the superconductor side approaches to the bulk value $\Delta(\phi_\alpha, \infty)$ at sufficiently large x . Hence, the evolution operator can be divided into a growing part and a decaying part:

$$U_\alpha(\phi_\alpha, x, x') = \Lambda_\alpha^{(+)}(\phi_\alpha, x, x') e^{\kappa_\alpha(x-x')} + \Lambda_\alpha^{(-)}(\phi_\alpha, x, x') e^{-\kappa_\alpha(x-x')}, \quad (14)$$

$$\begin{aligned} \Lambda_\alpha^{(+)}(\phi_\alpha, x, x') &= -\frac{1}{W_\alpha} \Phi_n^{(+)}(\phi_\alpha, x)^T \Phi_n^{(-)}(\phi_\alpha, x') \hat{\tau}_2, \\ \Lambda_\alpha^{(-)}(\phi_\alpha, x, x') &= \frac{1}{W_\alpha} \Phi_n^{(-)}(\phi_\alpha, x)^T \Phi_n^{(+)}(\phi_\alpha, x') \hat{\tau}_2, \end{aligned} \quad (15)$$

where

$$\begin{aligned} \kappa_\alpha &= \frac{\Omega_\alpha}{|v_{Fx}|}, \quad \Omega_\alpha = \sqrt{\omega_m^2 + |\Delta(\phi_\alpha, \infty)|^2}, \\ W_\alpha &= {}^T \Phi_n^{(+)}(\phi_\alpha, x) \hat{\tau}_2 \Phi_n^{(-)}(\phi_\alpha, x) = -{}^T \Phi_n^{(-)}(\phi_\alpha, x) \hat{\tau}_2 \Phi_n^{(+)}(\phi_\alpha, x) \\ &= \text{constant}. \end{aligned} \quad (16)$$

In the above, ${}^T \Phi_n^{(\alpha)}(\phi_\alpha, x)$ denotes the transposition of $\Phi_n^{(\alpha)}(\phi_\alpha, x)$.

Retaining the most divergent term in semi-infinite limit, we find the quasiclassical Green's function $\hat{g}_{\alpha\alpha}(\phi, x)$ in the superconductor side given by^{35,40},

$$\hat{g}_{\alpha\alpha}(\phi_\alpha, x) = i \left(\frac{2\hat{A}_{S\alpha}(x)}{\text{Tr}[\hat{A}_{S\alpha}(x)]} - 1 \right), \quad (17)$$

where

$$\begin{aligned} \hat{A}_{S+}(x) &= \Lambda_+^{(-)}(\phi_+, x, L) \Lambda_-^{(+)}(\phi_-, L, 0) \hat{R}_N U_+(\phi_+, 0, x) e^{-\kappa x} \\ &= \hat{\lambda}_{S+}(x, 0) \hat{R}_N \tilde{U}_+(\phi_+, 0, x), \end{aligned} \quad (18)$$

$$\hat{\lambda}_{S+}(x, 0) \propto \begin{pmatrix} u_n^{(-)}(\phi_+, x) \\ v_n^{(-)}(\phi_+, x) \end{pmatrix} \begin{pmatrix} u_n^{(-)}(\phi_-, 0) & v_n^{(-)}(\phi_-, 0) \end{pmatrix} \hat{\tau}_2. \quad (19)$$

In the above, the matrix \hat{R}_N represents resistance at the interface which is given by³⁸

$$\hat{R}_N \propto \begin{pmatrix} 1 & 0 \\ 0 & 1 - \sigma_N(\phi) \end{pmatrix}, \quad \sigma_N(\phi) = \frac{4 \cos \phi^2}{4 \cos \phi^2 + Z^2}, \quad (20)$$

where $\sigma_N(\phi)$ stands for tunneling conductance when the system is in the normal state⁴³ and Z is the effective barrier height at the interface with $Z = 2mH/(\hbar^2 k_F)$. In order to obtain the quantity $\tilde{U}_+(\phi_+, 0, x)$ in eq.(18), we rewrite $\hat{A}_{S+}(x)$ as⁴⁰

$$\hat{A}_{S+}(x) = \begin{pmatrix} u_n^{(-)}(\phi_+, x) \\ v_n^{(-)}(\phi_+, x) \end{pmatrix} \begin{pmatrix} X_+(x) & Y_+(x) \end{pmatrix} \hat{\tau}_2, \quad (21)$$

where $\mathcal{D}_\alpha(x) = (-i)v_n^{(-)}(\phi_\alpha, x)/u_n^{(-)}(\phi_\alpha, x)$ and $\mathcal{F}_+(x) = iX_+(x)/Y_+(x)$ obey the following Riccati type equations

$$\hbar|v_{Fx}| \frac{\partial}{\partial x} \mathcal{D}_\alpha(x) = \alpha \left[-2\omega_m \mathcal{D}_\alpha(x) + \Delta(\phi_\alpha, x) \mathcal{D}_\alpha^2(x) - \Delta^*(\phi_\alpha, x) \right], \quad (22)$$

$$\hbar|v_{Fx}| \frac{\partial}{\partial x} \mathcal{F}_+(x) = 2\omega_m \mathcal{F}_+(x) + \Delta^*(\phi_+, x) \mathcal{F}_+^2(x) - \Delta(\phi_+, x). \quad (23)$$

We can write the quasiclassical Green's function in a compact form³⁵,

$$\hat{g}_{++}(\phi_+, x) = i \left[\frac{2}{1 - \mathcal{D}_+(x) \mathcal{F}_+(x)} \begin{pmatrix} 1 & i\mathcal{F}_+(x) \\ i\mathcal{D}_+(x) & -\mathcal{D}_+(x) \mathcal{F}_+(x) \end{pmatrix} - 1 \right]. \quad (24)$$

Initial conditions of these equations are

$$\mathcal{D}_\alpha(\infty) = \frac{\Delta^*(\phi_\alpha, \infty)}{\omega_m + \alpha \Omega_\alpha}, \quad \mathcal{F}_+(0) = \frac{1 - \sigma_N(\phi)}{D_-(0)}. \quad (25)$$

The pair potential is given by^{25,39,40,38,33,34}

$$\Delta(\phi, x) = \sum_{0 \leq m < \omega_c / 2\pi T} \frac{1}{2\pi} \int_{-\pi/2}^{\pi/2} d\phi' \sum_{\alpha} V(\phi, \phi'_\alpha) [\hat{g}_{\alpha\alpha}(\phi'_\alpha, x)]_{12}, \quad (26)$$

with $\hat{g}_{--}(\phi_-, x) = -\hat{g}_{++}(-\phi_+, x)$, where ω_c is the cutoff energy and $[\hat{g}_{\alpha\alpha}(\phi_\alpha, x)]_{12}$ means the 12 element of $\hat{g}_{\alpha\alpha}(\phi_\alpha, x)$. Here $V(\phi, \phi_\alpha)$ is the effective inter-electron potential of the Cooper pair. In our numerical calculations, new $\Delta(\phi_\alpha, x)$ and $\hat{g}_{\alpha\alpha}(\phi_\alpha, x)$ are obtained using eqs.(22)-(24) and eq. (26). We repeat this iteration process until the sufficient convergence is obtained.

Next, we calculate the tunneling conductance spectra based on the self-consistently determined pair potential. The resulting normalized tunneling conductance $\sigma_T(eV)$ with the bias voltage V is given by^{31,43}

$$\sigma_T(eV) = \frac{\int_{-\pi/2}^{\pi/2} d\phi \int_{-\infty}^{\infty} dE \sigma_N(\phi) \sigma_S(E, \phi) \operatorname{sech}^2\left(\frac{E - eV}{2k_B T}\right) \cos \phi}{\int_{-\pi/2}^{\pi/2} d\phi \int_{-\infty}^{\infty} dE \sigma_N(\phi) \operatorname{sech}^2\left(\frac{E - eV}{2k_B T}\right) \cos \phi}, \quad (27)$$

$$\sigma_S(E, \phi) = \frac{1 + \sigma_N(\phi) |\Gamma_{S+}(E, \phi_+, 0)|^2 + [\sigma_N(\phi) - 1] |\Gamma_{S+}(E, \phi_+, 0)|^2 |\Gamma_{S-}(E, \phi_-, 0)|^2}{|1 + [\sigma_N(\phi) - 1] \Gamma_{S+}(E, \phi_+, 0) \Gamma_{S-}(E, \phi_-, 0)|^2}. \quad (28)$$

In the above, $\Gamma_{S\alpha}(E, \phi_\alpha, x)$ is obtained by solving following equations,

$$i\hbar |v_{Fx}| \frac{\partial}{\partial x} \Gamma_{S+}(E, \phi_+, x) = 2E \Gamma_{S+}(E, \phi_+, x) - \Delta(\phi_+, x) \Gamma_{S+}^2(E, \phi_+, x) - \Delta^*(\phi_+, x), \quad (29)$$

$$i\hbar |v_{Fx}| \frac{\partial}{\partial x} \Gamma_{S-}(E, \phi_-, x) = 2E \Gamma_{S-}(E, \phi_-, x) - \Delta^*(\phi_-, x) \Gamma_{S-}^2(E, \phi_-, x) - \Delta(\phi_-, x). \quad (30)$$

In the following, almost calculations are performed on the temperature $T/T_c = 0.05$, where T_c is the critical temperature of the bulk $d_{x^2-y^2}$ -wave superconductor.

III. BROKEN TIME REVERSAL SYMMETRY STATE NEAR AN INTERFACE OF A $D_{X^2-Y^2}$ -WAVE SUPERCONDUCTOR

In this section, the spatial dependence of the self-consistently determined pair potential and the corresponding tunneling conductance are presented for the $d_{x^2-y^2}$ -wave superconducting state. In the middle of the $d_{x^2-y^2}$ -wave superconductor, the pair potential is given by $\Delta(\phi_\alpha, \infty) = \Delta_0 \cos[2(\phi - \theta)]$, where θ is the angle between normal to the interface and the lobe direction of the $d_{x^2-y^2}$ -wave pair potential, *i.e.*, the angle between the x -axis and the crystal a -axis of the $d_{x^2-y^2}$ -wave. In this paper, we choose various θ ($0 \leq \theta \leq \pi/4$) by changing the magnitude of Z and T_s ($T_{d_{xy}}$).

A. $d_{x^2-y^2} + \text{is-wave state}$

In this subsection, we show the spatial dependence of the pair potential and the resulting tunneling conductance of the $d_{x^2-y^2} + \text{is-wave state}$ realized near the interface of the N/D

junction. The spatial dependence of the pair potential is expressed as

$$\Delta(\phi, x) = \Delta_d(x) \cos[2(\phi - \theta)] + \Delta_s(x), \quad (31)$$

where $\Delta_d(x)$ and $\Delta_s(x)$ correspond to the amplitude of the $d_{x^2-y^2}$ -wave and s -wave superconducting states, respectively. The attractive potential $V(\phi, \phi')$ is given by

$$V(\phi, \phi') = 2V_d \cos[2(\phi - \theta)] \cos[2(\phi' - \theta)] + V_s \quad (32)$$

where V_d and V_s denote the attractive potential of predominant $d_{x^2-y^2}$ -wave and subdominant s -wave, respectively, and they are given as

$$V_d = \frac{2\pi k_B T}{\log \frac{T}{T_c} + \sum_{0 \leq m < \omega_c/2\pi T} \frac{1}{m + 1/2}}, \quad (33)$$

$$V_s = \frac{2\pi k_B T}{\log \frac{T}{T_s} + \sum_{0 \leq m < \omega_c/2\pi T} \frac{1}{m + 1/2}}. \quad (34)$$

Here, T_s denotes the transition temperature of s -wave component of the pair potential without predominant $d_{x^2-y^2}$ -wave component. For $\theta = 0$ or $\theta = \pi/4$, only $\text{Re}[\Delta_d(x)]$ and $\text{Im}[\Delta_s(x)]$ are nonzero. The spatial dependence of the pair potentials $\text{Re}[\Delta_d(x)]$ and $\text{Im}[\Delta_s(x)]$ is plotted in Fig. 1(a) for various θ with $T_s/T_d = 0.2$ and $Z = 3$. The x -axis of Fig. 1(a) is normalized by $\xi_0 = \hbar v_F/\Delta_0$ which is the coherence length of the superconductor. For $\theta = 0$ [(100) surface], since $\text{Im}[\Delta_s(x)] = 0$ is satisfied, the time reversal symmetry is not broken and the amplitude of $\text{Re}[\Delta_d(x)]$ is not suppressed at the interface. By changing the angle θ from zero, the magnitude of $\text{Re}[\Delta_d(x)]$ is reduced near the interface, while $\text{Im}[\Delta_s(x)]$ is induced at the interface²⁵. The suppression of $\text{Re}[\Delta_d(x)]$ is originated from a depairing effect that the effective pair potentials $\Delta(\phi_+, 0)$ and $\Delta(\phi_-, 0)$ have reversed contribution to the pairing interaction for certain range of ϕ for $\theta \neq 0$. When $\text{Re}[\Delta_d(x)]$ is suppressed at the interface, the quasiparticle forms the ABS near the interface at zero-energy⁵. The ABS is unstable with the introduction of s -wave attractive potential, then $\text{Im}[\Delta_s(x)]$ is induced at the interface²⁵. The magnitude of $\text{Im}[\Delta_s(x)]$ becomes maximum at $\theta = \pi/4$, where the

above suppression effect is most significant. In Fig. 1(b), $\text{Re}[\Delta_d(x)]$ and $\text{Im}[\Delta_s(x)]$ are plotted for various Z with $T_s/T_d = 0.2$ and $\theta = \pi/4$. Even if the BTRSS becomes to be most stable at $\theta = \pi/4$, when the height of barrier is small, the magnitude of the subdominant imaginary component of $\Delta_s(x)$ is not induced at all. The induced imaginary component of $\Delta_s(x)$ is enhanced with the increase of Z .

The spatial dependence of the pair potentials near the interface with the intermediate angle ($\theta = \pi/6$) is shown in Fig. 2 for various height of barrier. In such a case, both $\text{Im}[\Delta_d(x)]$ and $\text{Re}[\Delta_s(x)]$ becomes nonzero and the spatial dependence is much more complex as compared to that for $\theta = 0$ or $\theta = \pi/4$. The amplitudes of $\text{Im}[\Delta_d(x)]$, $\text{Re}[\Delta_s(x)]$, and $\text{Im}[\Delta_s(x)]$ are enhanced for larger magnitude of Z , where the suppression of $\text{Re}[\Delta_d(x)]$ is significant. However, the amplitudes of $\text{Im}[\Delta_d(x)]$ and $\text{Re}[\Delta_s(x)]$ are one order smaller than that of $\text{Im}[\Delta_s(x)]$.

Next, we look at the magnitude of subdominant components of the pair potential at the interface, $\text{Im}[\Delta_s(0)]$, $\text{Im}[\Delta_d(0)]$, and $\text{Re}[\Delta_s(0)]$, for various T_s , Z , and θ . As shown in Fig. 3(a), the magnitude of $\text{Im}[\Delta_s(0)]$ increases monotonically with T_s for fixed θ and Z , and it is enhanced for larger magnitude of Z . In other words, the amplitude of $\text{Im}[\Delta_s(0)]$ is sensitive to the transmission probability of the junctions. In Fig. 3(b), $\text{Im}[\Delta_s(0)]$ is plotted as a function of θ for sufficiently larger magnitude of $Z(= 5.0)$. For $\theta = 0$, *i.e.*, junction with (100) interface, the magnitude of $\text{Im}[\Delta_s(0)]$ is negligibly small near the interface even at the larger magnitude of T_s . The magnitude of $\text{Im}[\Delta_s(0)]$ is a monotonically increasing function with the increase of θ and has a maximum at $\theta = \pi/4$. As seen from Figs. 3(c) and 3(d), both the magnitude of $\text{Im}[\Delta_d(0)]$ and $\text{Re}[\Delta_s(0)]$ is enhanced and has a maximum at a certain θ . In the intermediate θ , *i.e.*, $\theta \neq 0$ or $\theta \neq \pi/4$, the magnitude of $\Delta(\phi_+, x)$ and that of $\Delta(\phi_-, x)$ does not coincide any more, the interference with the quasiparticle and the pair potential becomes complex. Then, not only $\text{Im}[\Delta_s(0)]$ but also $\text{Re}[\Delta_s(0)]$ and $\text{Im}[\Delta_d(0)]$ become nonzero.

Using self-consistently determined pair potentials, let us look at the normalized tunneling conductance $\sigma_T(eV)$. In order to clarify the temperature T dependence of $\sigma_T(eV)$, we choose

$T = 0$ in the left panels of Fig. 4 and $T = 0.05T_c$ in the right panels. Only for $\theta = 0$, line shape of $\sigma_T(eV)$ is similar to that of the bulk density of states of $d_{x^2-y^2}$ -wave superconducting state. In other cases, $\sigma_T(eV)$ has a zero bias enhanced line shape. As clarified in previous literatures⁴, when θ deviates from zero, since the injected and reflected quasiparticles have a chance to feel the sign change of the pair potentials, zero-energy ABS is formed at the interface. This zero-energy ABS causes the ZBCP when the magnitude of T_s is small. With the increase of the magnitude of T_s , the zero energy ABS is unstable and s -wave subdominant component is induced which breaks time reversal symmetry and it blocks the motion of the quasiparticles. Then, the energy levels of bound state shift from zero and the local density of states has a zero-energy peak splitting. The resulting $\sigma_T(eV)$ has a ZBCP splitting as shown in Fig. 4(b). However, with the increase of T , the slight splitting of ZBCP fades out due to smearing effect by finite temperature and the resulting $\sigma_T(eV)$ has a rather broad ZBCP [see Fig. 4(c) and Fig. 4(d)].

Next, we concentrate on how $\sigma_T(eV)$ is influenced by the transmission probability of the junctions, *i.e.*, the magnitude of Z . In Fig. 5, $\sigma_T(eV)$ with $\theta = \pi/4$ is plotted for $T = 0$ (left panels) and $T = 0.05T_c$ (right panels). For the junctions with high transmissivity, $\sigma_T(eV)$ has a ZBCP, [see Fig. 5(a)] and the magnitude of $\sigma_T(0)$ is firstly enhanced with the increase of Z . In this case, the predominant $d_{x^2-y^2}$ -wave component only exists near the interface as shown in Fig. 1(b). However, with the increase of Z , $\sigma_T(eV)$ starts to have a ZBCP splitting at a certain value of Z , where the magnitude of subdominant component $\text{Im}[\Delta_s(x)]$ at the interface becomes the same order as that of the predominant component $\text{Re}[\Delta_d(x)]$. For sufficiently larger magnitude of Z , $\sigma_T(eV)$ has a ZBCP splitting, [see Fig. 5(b) and 5(c),] and the magnitude of $\sigma_T(0)$ decreases with the increase of Z . However, the above obtained results are influenced by finite temperature effect. The right panels of Fig. 5 is shown for the tunneling conductance in $T/T_c = 0.05$. The slight enhanced structure of $\sigma_T(eV)$ at $eV = \pm\Delta_0$ in Fig. 5(a), 5(b), and 5(c) is invisible due to the smearing effect by finite temperature [see Fig. 5(c), 5(d), and 5(e)]. With the increase of the magnitude of Z , $\sigma_T(eV)$ has a ZBCP with tiny dip even at $Z = 2.5$, where the order of the amplitude of $\text{Im}[\Delta_s(0)]$ is

$0.2\Delta_0$. With the further increase of Z , $\sigma_T(eV)$ has a ZBCP splitting [see Fig. 5(f)], however the degree of the splitting is significantly weakened as compared to the corresponding curves in Fig. 5(c).

Finally, we look at the relation between the position of the splitted peak and the magnitude of $\text{Im}[\Delta_s(0)]$. In Fig. 6(a), $\sigma_T(eV)$ is plotted for various T_s with $Z = 5$ and $T = 0$. As shown in Fig. 3(b), the magnitude of the induced subdominant imaginary component of $\text{Im}[\Delta_s(0)]$ is about $0.16\Delta_0$, $0.3\Delta_0$, and $0.42\Delta_0$ for $T_s/T_d = 0.1$, $T_s/T_d = 0.3$ and $T_s/T_d = 0.5$, respectively. The corresponding $\sigma_T(eV)$ has a splitted peak locating at $\pm 0.16\Delta_0$, $\pm 0.3\Delta_0$, and $\pm 0.42\Delta_0$, respectively. With the increase of T , the height of these peaks are drastically suppressed as shown in Fig. 6(b). Finally, we show how the line shape of $\sigma_T(eV)$ changes at the temperature $T = T_{\bar{s}}$ ($T_{\bar{s}} = 0.12T_c$) where $\text{Im}[\Delta_s(x)]$ becomes nonzero. As seen from Fig. 6(c), the magnitude of $\sigma_T(0)$ is reduced with the introduction of $\text{Im}[\Delta_s(x)]$.

At the end of this subsection, we can summarize that even in the presence of BTRSS, the resulting $\sigma_T(eV)$ does not always have a clear ZBCP splitting due to the finite temperature effect when the magnitude of the transmission probability of the junctions is not low.

B. $d_{x^2-y^2}+id_{xy}$ -wave state

In this subsection, we study spatial dependence of the pair potentials of the $d_{x^2-y^2}+id_{xy}$ -wave state and the resulting tunneling conductance in N/D junctions. The pair potential is given by

$$\Delta(\phi, x) = \Delta_d(x) \cos[2(\phi - \theta)] + \Delta_{d_{xy}}(x) \sin[2(\phi - \theta)], \quad (35)$$

where $\Delta_{d_{xy}}(x)$ is an amplitude of the d_{xy} -wave superconducting state and a complex number. The attractive inter-electron potential $V(\phi, \phi')$ is given by

$$V(\phi, \phi') = 2V_d \cos[2(\phi - \theta)] \cos[2(\phi' - \theta)] + 2V_{d_{xy}} \sin[2(\phi - \theta)] \sin[2(\phi' - \theta)], \quad (36)$$

where V_d and $V_{d_{xy}}$ stand for the attractive potential of predominant $d_{x^2-y^2}$ -wave and subdominant d_{xy} -wave, respectively, and they are given as

$$V_d = \frac{2\pi k_B T}{\log \frac{T}{T_c} + \sum_{0 \leq m < \omega_c / 2\pi T} \frac{1}{m + 1/2}}, \quad (37)$$

$$V_{d_{xy}} = \frac{2\pi k_B T}{\log \frac{T}{T_{d_{xy}}} + \sum_{0 \leq m < \omega_c / 2\pi T} \frac{1}{m + 1/2}}. \quad (38)$$

The spatial dependence of the pair potentials with a finite transmissivity for $Z = 3.0$ and $\theta = \pi/4$ is shown in Fig. 7(a). As in the case for $d_{x^2-y^2}+is$ -wave state, the amplitude of $\text{Im}[\Delta_{d_{xy}}(x)]$ vanishes at $\theta = 0$. For $\theta = \pi/4$, the suppression of the magnitude of $\text{Re}[\Delta_d(x)]$ is most significant, while $\Delta_{d_{xy}}(x)$ is induced at the interface. At this θ , the d_{xy} -wave component is not affected by depairing effect seriously since the lobe direction of d_{xy} -wave pair potential is parallel or perpendicular to the interface as in the case for predominant $d_{x^2-y^2}$ -wave with $\theta = 0$. As shown in Fig. 7(b), the amplitude of $\text{Im}[\Delta_{d_{xy}}(x)]$ is enhanced with the increase of Z .

The spatial dependencies of $\text{Re}[\Delta_d(x)]$, $\text{Im}[\Delta_d(x)]$, $\text{Re}[\Delta_s(x)]$, and $\text{Im}[\Delta_s(x)]$ are plotted in Figs. 8(a), 8(b), 8(c), and 8(d), respectively, with the intermediate θ ($\theta = \pi/6$) for various Z . In such a case, the spatial dependence is much more complex as compared to that for $\theta = 0$ or $\theta = \pi/4$, and both $\text{Im}[\Delta_d(x)]$ and $\text{Re}[\Delta_{d_{xy}}(x)]$ become nonzero. The amplitudes of $\text{Im}[\Delta_d(x)]$, $\text{Re}[\Delta_{d_{xy}}(x)]$, and $\text{Im}[\Delta_s(x)]$ are enhanced for larger magnitude of Z , where the suppression of $\text{Re}[\Delta_d(x)]$ is significant. The remarkable feature is that the amplitude of $\text{Im}[\Delta_d(x)]$ and $\text{Re}[\Delta_{d_{xy}}(x)]$ can become the same order of $\text{Im}[\Delta_s(x)]$ for larger Z .

Next, we look at the magnitude of subdominant components of the pair potential at the interface, $\text{Im}[\Delta_{d_{xy}}(0)]$, $\text{Im}[\Delta_d(0)]$, and $\text{Re}[\Delta_{d_{xy}}(0)]$ for various parameters $T_{d_{xy}}$, Z and θ shown in Fig. 9. The magnitude of $\text{Im}[\Delta_{d_{xy}}(0)]$ increases monotonically with $T_{d_{xy}}$ for fixed θ and Z . It is also enhanced for larger magnitude of Z . Comparing the corresponding situation of $d_{x^2-y^2} + is$ -wave shown in Fig. 3(a), the magnitude of $\text{Im}[\Delta_{d_{xy}}(0)]$ is suppressed for the small magnitude of $T_{d_{xy}}$. In Fig. 9(b), $\text{Im}[\Delta_{d_{xy}}(0)]$ is plotted as a function of θ for sufficiently larger magnitude of Z ($= 5.0$). The magnitude of $\text{Im}[\Delta_{d_{xy}}(0)]$ is a monotonically increasing function with the increase of θ and has a maximum at $\theta = \pi/4$. The amplitudes of

$\text{Im}[\Delta_d(0)]$ and $\text{Re}[\Delta_{d_{xy}}(0)]$ are negligibly small for $\theta = 0$ and $\theta = \pi/4$, and has a maximum at a certain θ as shown in Figs. 9(c) and 9(d), respectively.

The resulting normalized tunneling conductance $\sigma_T(eV)$ is plotted in Figs. 10(a) and 10(b) with $T = 0$ and the corresponding quantities with $T = 0.05T_c$ is plotted in Figs. 10(c) and 10(d) for various θ . Only for $\theta = 0$, line shape of $\sigma_T(eV)$ is similar to that of the bulk density of states of $d_{x^2-y^2}$ -wave superconducting state. In other cases, $\sigma_T(eV)$ has a zero-bias enhanced line shape due to the formation of ABS [see Fig. 4(a)]. The ABS causes the ZBCP when the magnitude of $T_{d_{xy}}$ is small. However, with the increase of the magnitude of $T_{d_{xy}}$, the zero-energy ABS is unstable and subdominant d_{xy} -wave component is induced. The energy levels of bound state shifts from zero and the local density of states has a zero-energy peak splitting. The resulting $\sigma_T(eV)$ has a ZBCP splitting as shown in Fig. 10(b). As compared to the case of $d_{x^2-y^2}$ -wave state, the magnitude of $\sigma_T(0)$ is not reduced seriously since the effective d_{xy} -wave pair potential felt by quasiparticles is distributed from $-\text{Im}[\Delta_{d_{xy}}(0)]$ to $\text{Im}[\Delta_{d_{xy}}(0)]$. With the increase of temperature, the ZBCP splitting is not visible any more. [see Fig. 10(c) and Fig. 10(d)].

Next, we concentrate on how $\sigma_T(eV)$ is influenced by the transmissivity of the junctions, *i.e.*, the magnitude of Z . In Fig. 11, $\sigma_T(eV)$ with $\theta = \pi/4$ is plotted for $T = 0$ (left panels) and $T = 0.05T_c$ (right panels). As shown in Fig. 11, $\sigma_T(eV)$ with $\theta = \pi/4$ depends on the transmissivity of the junction crucially. For the junctions with high transmissivity, $\sigma_T(eV)$ has a ZBCP [see Fig. 11(a)] and the magnitude of $\sigma_T(0)$ is firstly enhanced with the increase of Z . In this case, only the predominant $d_{x^2-y^2}$ -wave component exists near the interface as shown in Fig. 1(b). However, with the increase of Z , $\sigma_T(eV)$ starts to have a peak splitting at a certain value of Z , where the magnitude of the induced subdominant component at the interface $\text{Im}[\Delta_{d_{xy}}(0)]$ overlaps that of the predominant one $\text{Re}[\Delta_d(x)]$. For sufficiently larger magnitude of Z , $\sigma_T(eV)$ has a ZBCP splitting [see Figs. 11(b) and 11(c)] and the magnitude of $\sigma_T(0)$ decreases with the increase of Z . The right panels of Fig. 11 are shown for the $\sigma_T(eV)$ with finite temperature. Only for the junctions with the lowest transmissivity ($Z = 5$), the subtle splitting of ZBCP appears in $\sigma_T(eV)$. For $T = 0.05T_c$,

similar line shapes of $\sigma_T(eV)$ with smeared ZBCP splitting are obtained [see Fig. 11(d), Fig. 11(e) and Fig. 11(f)]. However, the slight enhanced structure of $\sigma_T(eV)$ at $eV = \pm\Delta_0$ vanishes.

Finally, we look at the relation between the position of the splitted peak and the magnitude of $\text{Im}[\Delta_{d_{xy}}(0)]$. In Fig. 12(a), we show $T_{d_{xy}}$ dependence of the tunneling conductance spectra $\sigma_T(eV)$ for $\theta = 0$ with $Z = 5$. As shown in Fig. 9(b), the magnitude of the induced subdominant imaginary component of $\text{Im}[\Delta_{d_{xy}}(0)]$ is about $0.15\Delta_0$, $0.35\Delta_0$, and $0.52\Delta_0$ for $T_{d_{xy}}/T_d = 0.1$, $T_{d_{xy}}/T_d = 0.3$ and $T_{d_{xy}}/T_d = 0.5$, respectively. The corresponding $\sigma_T(eV)$ has a splitted peak locating at $\pm 0.16\Delta_0$, $\pm 0.3\Delta_0$, and $\pm 0.42\Delta_0$, respectively. The width of the two splitted peaks depends on the temperature as shown in Fig. 12(b). Next, we show how the line shape of $\sigma_T(eV)$ changes at the temperature $T = T_{d_{xy}}^-$ [$T_{d_{xy}}^- = 0.07T_c$] where $\text{Im}[\Delta_{d_{xy}}(x)]$ becomes nonzero. As seen from Fig. 12(c), the magnitude of $\sigma_T(0)$ is reduced with the introduction of $\text{Im}[\Delta_s(x)]$.

At the end of this section, we can summarize that even in the presence of BTRSS, the resulting $\sigma_T(eV)$ does not always have a clear ZBCP splitting due to the finite temperature effect when the transmission probability of the particles at the interface is not low. In order to observe the ZBCP splitting which is one of the evidence supporting BTRSS, we must measure $\sigma_T(eV)$ for the junctions with low transmissivity with (110) oriented interface ($\theta = \pi/4$) at low temperatures. In such a case, we can classify the the $d_{x^2-y^2+is}$ - and $d_{x^2-y^2+id_{xy}}$ -wave state through the magnitude of $\sigma_T(0)$ and the width of the ZBCP splitting for the junctions with low transmission probability.

IV. CONCLUSION

In this paper, spatial dependence of the pair potential in the N/D junctions is determined on the basis of the quasiclassical theory in the presence of subdominant component of the pair potential near the interface. We clarified the influence of the spatial variation of the pair potentials on the tunneling conductance spectra for various conditions of the junctions.

We selected two kinds of subdominant components s - and d_{xy} -wave which are induced as $d_{x^2-y^2}+is$ - and $d_{x^2-y^2}+id_{xy}$ -wave state, respectively. The amplitude of $\Delta_s(x)$ [$\Delta_{d_{xy}}(x)$] is enhanced with the increase of the magnitude of Z , T_s [$T_{d_{xy}}$], and θ ($0 < \theta < \pi/4$). In the intermediate θ , both $\text{Im}[\Delta_d(x)]$ and $\text{Re}[\Delta_s(x)]$ $\{\text{Re}[\Delta_{d_{xy}}]\}$ becomes nonzero, although these magnitudes are small as compared to those of $\text{Re}[\Delta_d(x)]$ and $\text{Im}[\Delta_s(x)]$ $\{\text{Im}[\Delta_{d_{xy}}]\}$. The resulting $\sigma_T(eV)$ depends on Z , T_s (or $T_{d_{xy}}$), and θ . For fixed Z , the magnitude of $\sigma_T(0)$ increases with the increase of θ ($0 < \theta < \pi/4$) for small magnitude of T_s/T_d [$T_{d_{xy}}/T_d$]. While $\sigma_T(0)$ increases and decreases again with the increase of θ ($0 < \theta < \pi/4$) due to the formation of $d_{x^2-y^2}+is$ - [$d_{x^2-y^2}+id_{xy}$]-wave state for sufficiently larger magnitude of T_s/T_d [$T_{d_{xy}}/T_d$]. For fixed θ and T_s/T_d [$T_{d_{xy}}/T_d$], $\sigma_T(eV)$ has a ZBCP for small magnitude of Z , while it has a ZBCP splitting for sufficiently larger magnitude of Z . Using junctions with small transmissivity, we can distinguish $d_{x^2-y^2}+is$ -wave state from $d_{x^2-y^2}+id_{xy}$ -wave state since the magnitude of $\sigma_T(0)$ for $d_{x^2-y^2}+is$ -wave state is much more reduced as compared to that for $d_{x^2-y^2}+id_{xy}$ -wave state as seen from Fig. 4 [Fig. 6] to Fig. 10 [Fig. 12]. By taking into account finite temperature effect, the degree of the ZBCP splitting is suppressed and the fine structure at $eV \sim \Delta_0$ in $\sigma_T(eV)$ becomes invisible.

In the light of our theory, one of the reason for the absence of ZBCP splitting for many tunneling experiments may be due to their high transmissivity of the junctions (small magnitude of Z) and high temperatures. If we choose T_c as 90K, unless the transmissivity of the junction is sufficiently low, it is difficult to observe ZBCP splitting clearly at 4.5K. In order to see the ZBCP splitting clearly, we must observe much more low temperature ($T < 4.5K$) using a clean junctions with low transmissivity for $\theta = \pi/4$.

In this paper, we have chosen a free electron model with cylindrical Fermi surfaces. In order to compare actual tunneling conductance, we must calculate spatial dependence of the pair potential and the tunneling conductance by taking into account of the actual shape of Fermi surface. For this purpose, it is a promising way to perform the calculation based on the t - J model with Gutzwiller approximation⁴⁴, where the doping dependence is naturally taken into account. Using this model, we succeeded to explain detailed line shape of the scanning

tunneling conductance spectra around Zn impurity^{45–47}. As regards quasiparticle states near the interface, the pre-existing calculations are performed for infinite barrier limit^{10,28,29}. In order to compare actual tunneling experiments, we must calculate the N/D junctions based on the t - J model using Gutzwiller approximation. In the t - J model, the subdominant d_{xy} -wave component is hard to be realized⁴⁴ since a nearest neighbor attractive potential is taken into account. In order to discuss the d_{xy} -wave component, we must consider much more long range interaction including three site hopping term.

It is also revealed by recent theory that the BTRSS influences significantly on the Josephson effect^{48–50}. The previous theory assumes a sufficient larger magnitude of barrier⁵⁰. In order to compare the existing experiments, we must calculate Josephson current in the presence of BTRSS for arbitrary transmissivity of the junctions.

ACKNOWLEDGMENTS

First author (Y.T.) would like to thank K. Machida and M. Ichioka for useful and fruitful discussions. He acknowledges the financial support of Research Fellowships of Japan Society for the Promotion of Science (JSPS) for Young Scientists. This work is supported by the Core Research for Evolutional Science and Technology (CREST) of the Japan Science and Technology Corporation (JST). The computational aspect of this work has been performed at the facilities of the Supercomputer Center, Institute for Solid State Physics, University of Tokyo and the Computer Center.

REFERENCES

* Present address: Department of Physics, Okayama University, Okayama, 700-8530, Japan

- ¹ D. J. Scalapino, Phys. Rep. **250** 329 (1995).
- ² M. Sigrist and T. M. Rice, J. Phys. Soc. Jpn. **61** 4283 (1992); Rev. Mod. Phys. **67** 505 (1995).
- ³ D. J. Van Harlingen, Rev. Mod. Phys. **67** 515 (1995).
- ⁴ S. Kashiwaya and Y. Tanaka, Rep. Prog. Phys. **63** 1641 (2000).
- ⁵ C. R. Hu, Phys. Rev. Lett. **72** 1526 (1994).
- ⁶ Y. Tanaka and S. Kashiwaya, Phys. Rev. Lett. **74** 3451 (1995).
- ⁷ S. Kashiwaya, Y. Tanaka, M. Koyanagi, H. Takashima, and K. Kajimura, Phys. Rev. B **51** 1350 (1995).
- ⁸ Y. Nagato and K. Nagai, Phys. Rev. B **51** 16254 (1995).
- ⁹ S. Kashiwaya, Y. Tanaka, M. Koyanagi, and K. Kajimura, Phys. Rev. B **53** 2667 (1996).
- ¹⁰ Y. Tanuma, Y. Tanaka, M. Yamashiro, and S. Kashiwaya, Phys. Rev. B. **57** 7997 (1998).
- ¹¹ L. Alff, H. Takashima, S. Kashiwaya, N. Terada, H. Ihara, Y. Tanaka, M. Koyanagi, and K. Kajimura, Phys. Rev. B **55** 14757 (1997).
- ¹² J. Y. T. Wei, N.-C. Yeh, D. F. Garrigus, and M. Strasik, Phys. Rev. Lett. **81** 2542 (1998).
- ¹³ N.C. Yeh, J.Y.T. Wei, C.T. Chen, W.D. Si, and X.X. Xi, Physica C **341-348** 1639 (2000).
- ¹⁴ W. Wang, M. Yamazaki, K. Lee, and I Iguchi, Phys. Rev. B **60** 4272 (1999).
- ¹⁵ I. Iguchi, W. Wang, M. Yamazaki, Y. Tanaka, and S. Kashiwaya, Phys. Rev. B **62** R6131 (2000).
- ¹⁶ M. Sigrist, D. B. Bailey, and R. B. Laughlin, Phys. Rev. Lett. **74** 3249 (1995).

- ¹⁷ K. Kuboki and M. Sigrist, J. Phys. Soc. Jpn. **65** 361 (1996).
- ¹⁸ M. Sigrist, Prog. Theo. Phys. **99** 899 (1998).
- ¹⁹ K. Krishana, N. P. Ong, Q. Li, G. D. Gu, and N. Koshizuka, Science **277** 83 (1997).
- ²⁰ A. V. Balatsky, Phys. Rev. Lett. **80** 1972 (1998).
- ²¹ R. B. Laughlin, Phys. Rev. Lett. **80** 5188 (1998).
- ²² M. Covington, M. Aprili, E. Paraoanu, L. H. Greene, F. Xu, J. Zhu, and C. A. Mirkin, Phys. Rev. Lett. **79** 277 (1997).
- ²³ R. Krupke and G. Deutscher, Phys. Rev. Lett. **83** 4634 (2000).
- ²⁴ A. Sharoni, G. Koren, and O. Millo, cond-mat/0103581.
- ²⁵ M. Matsumoto and H. Shiba, J. Phys. Soc. Jpn. **64** 3384 (1995); *ibid.* **64** 4867 (1995), *ibid.* **65** 2194 (1996).
- ²⁶ M. Fogelström, D. Rainer, and J. A. Sauls, Phys. Rev. Lett. **79** 281 (1997).
- ²⁷ D. Rainer, H. Burkhardt, M. Fogelström, and J. A. Sauls, J. Phys. Chem. Solid. **59** 2040 (1998).
- ²⁸ Y. Tanuma, Y. Tanaka, M. Ogata, and S. Kashiwaya, J. Phys. Soc. Jpn. **67** 1118 (1998); Phys. Rev. B **60** 9817 (1999).
- ²⁹ J. X. Zhu and C. S. Ting, Phys. Rev. B **59** 14165 (1999).
- ³⁰ The existence of ferromagnetic layer near the interface of *d*-wave superconductor also induces ZBCP splitting. S. Kashiwaya, Y. Tanaka, N. Yoshida, and M. R. Beasley, Phys. Rev. B **60** 3572 (1999); J. X. Zhu, B. Friedman and C. S. Ting, Phys. Rev. B **59** 9558 (1999).
- ³¹ Y. Tanaka, Y. Tanuma, and S. Kashiwaya, Phys. Rev. B (2001).

- ³² G. Eilenberger, Z. Phys. **214** 195 (1968).
- ³³ C. Bruder, Phys. Rev. B **41** 4017 (1990).
- ³⁴ Y. Ohashi, J. Phys. Soc. Jpn. **65** 823 (1996).
- ³⁵ K. Nagai, *Quasiclassical Methods in Superconductivity and Superfluidity*, ed. D. Rainer and J. A. Sauls (unpublished).
- ³⁶ L. J. Buchholtz, M. Palumbo, D. Rainer, and J. A. Sauls, J. Low. Temp. Phys. **101** 1079 (1995); *ibid.* **101** 1097 (1995).
- ³⁷ Y. S. Barash, A. A. Svidzinsky, and H. Burkhardt, Phys. Rev. B **55** 15282 (1997).
- ³⁸ M. Yamashiro, Y. Tanaka, N. Yoshida, and S. Kashiwaya, J. Phys. Soc. Jpn. **68** 2019 (1999).
- ³⁹ M. Ashida, S. Aoyama, J. Hara, and K. Nagai, Phys. Rev. B **40** 8673 (1989).
- ⁴⁰ Y. Nagato, K. Nagai, and J. Hara, J. Low Temp. Phys. **93** 33 (1993).
- ⁴¹ P. G. de Gennes, *Superconductivity of Metals and Alloys* (Benjamin, New York, 1966).
- ⁴² J. Kurkijarvi and D. Rainer, *Helium Three*, ed. W. P. Halperin and L. P. Pitaevskii (Elsevier, Amsterdam, 1990).
- ⁴³ M. Yamashiro, Y. Tanaka, Y. Tanuma, and S. Kashiwaya, J. Phys. Soc. Jpn. **67** 3224 (1998).
- ⁴⁴ H. Yokoyama and M. Ogata, J. Phys. Soc. Jpn. **65** 3615 (1996).
- ⁴⁵ S. H. Pan, E. W. Hudson, K. M. Lang, H. Eisaki, S. Uchida, and J. C. Davis, Nature **403** 746 (2000).
- ⁴⁶ H. Tsuchiura, Y. Tanaka, M. Ogata, and S. Kashiwaya, J. Phys. Soc. Jpn. **68** 2510 (1999).
- ⁴⁷ H. Tsuchiura, Y. Tanaka, M. Ogata, and S. Kashiwaya, Phys. Rev. Lett. **84** 3165 (2000).

⁴⁸ Y. Tanaka and S. Kashiwaya, Phys. Rev. B **53** 11957 (1996); Phys. Rev. B **56** 892 (1997).

⁴⁹ Y. S. Barash, H. Burkhardt, and D. Rainer, Phys. Rev. Lett. **77** 4070 (1996).

⁵⁰ Y. Tanaka and S. Kashiwaya, Phys. Rev. B **58** 2948 (1998).

FIGURES

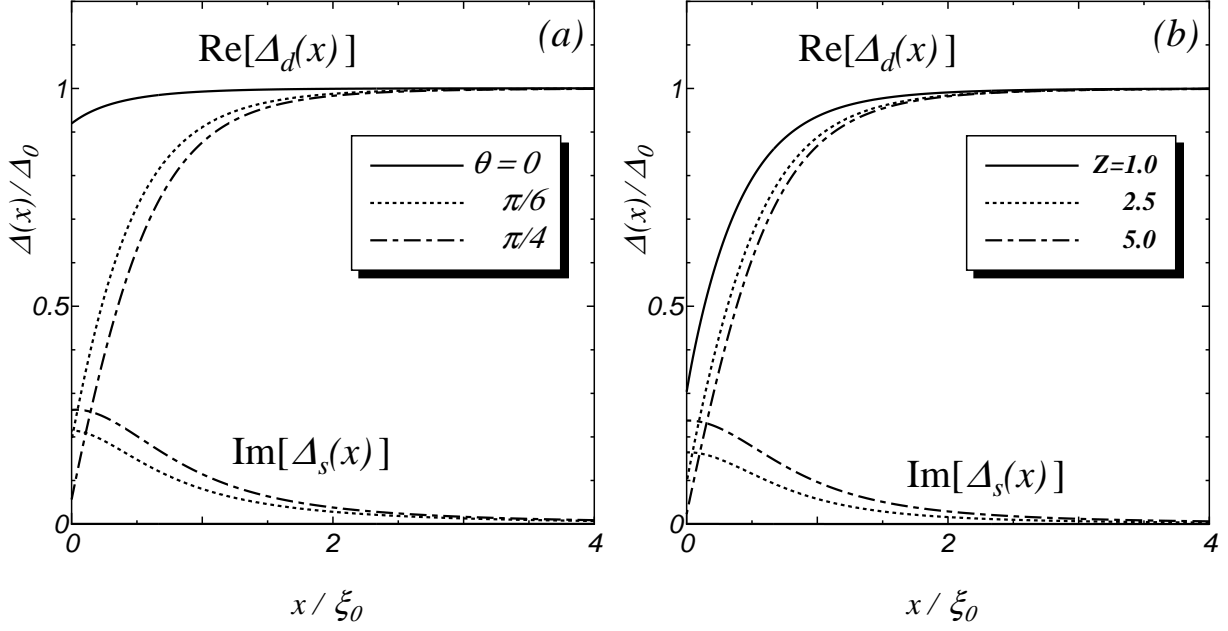


FIG. 1. Spatial dependences of the pair potential at $T_s/T_d = 0.2$; (a) near the interface for the angle θ between x -axis and crystal axis at $Z = 3.0$, and (b) near the (110) interface [$\theta = \pi/4$] for various height of barrier Z . $T = 0.05T_c$.

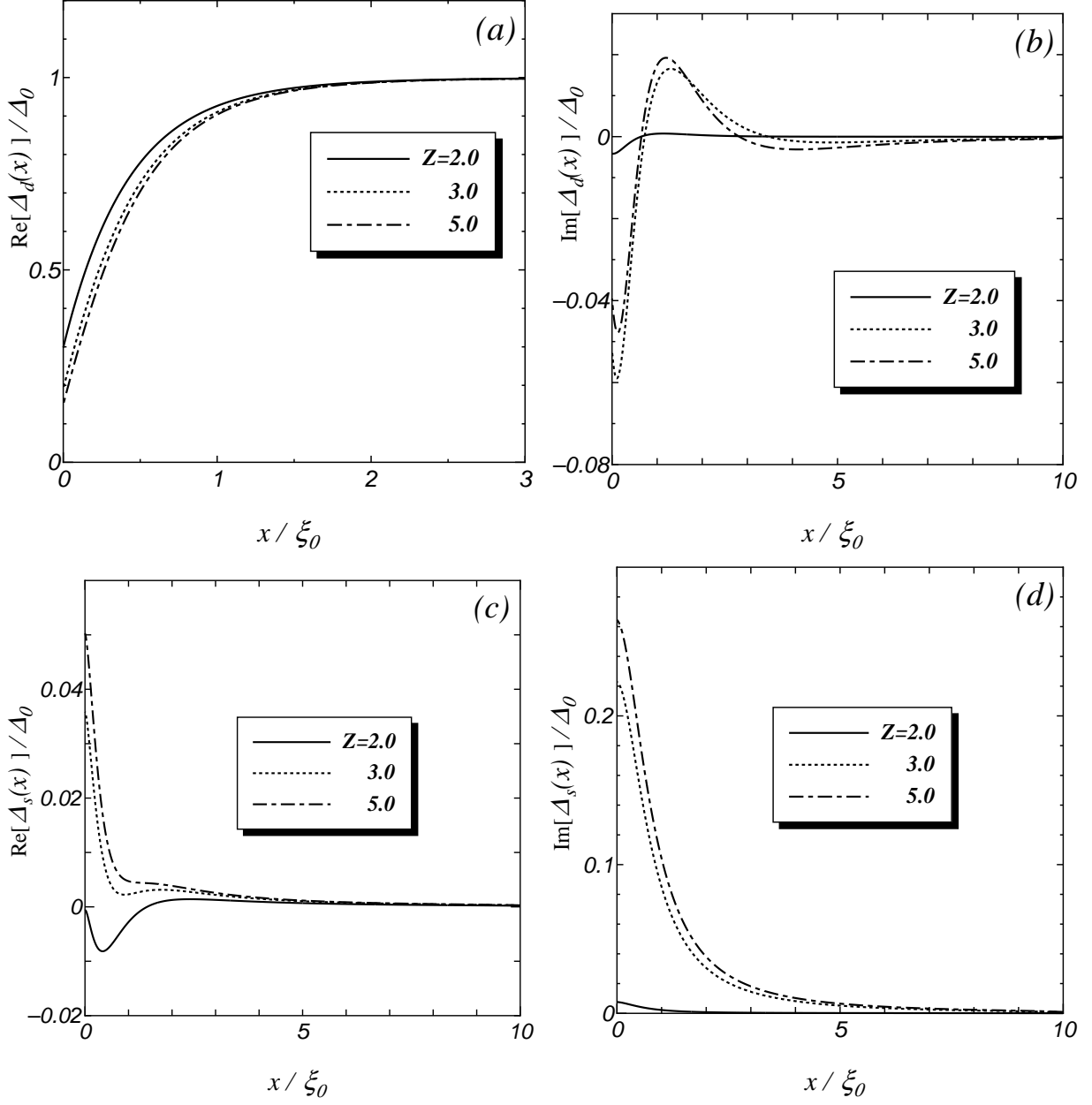


FIG. 2. Spatial dependence of the pair potentials near the interface with $\theta = \pi/6$ and $T_s/T_d = 0.3$; (a) real part of $\Delta_d(x)$, (b) imaginary part of $\Delta_d(x)$, (c) real part of $\Delta_s(x)$, and (d) imaginary part of $\Delta_s(x)$. $T = 0.02T_c$.

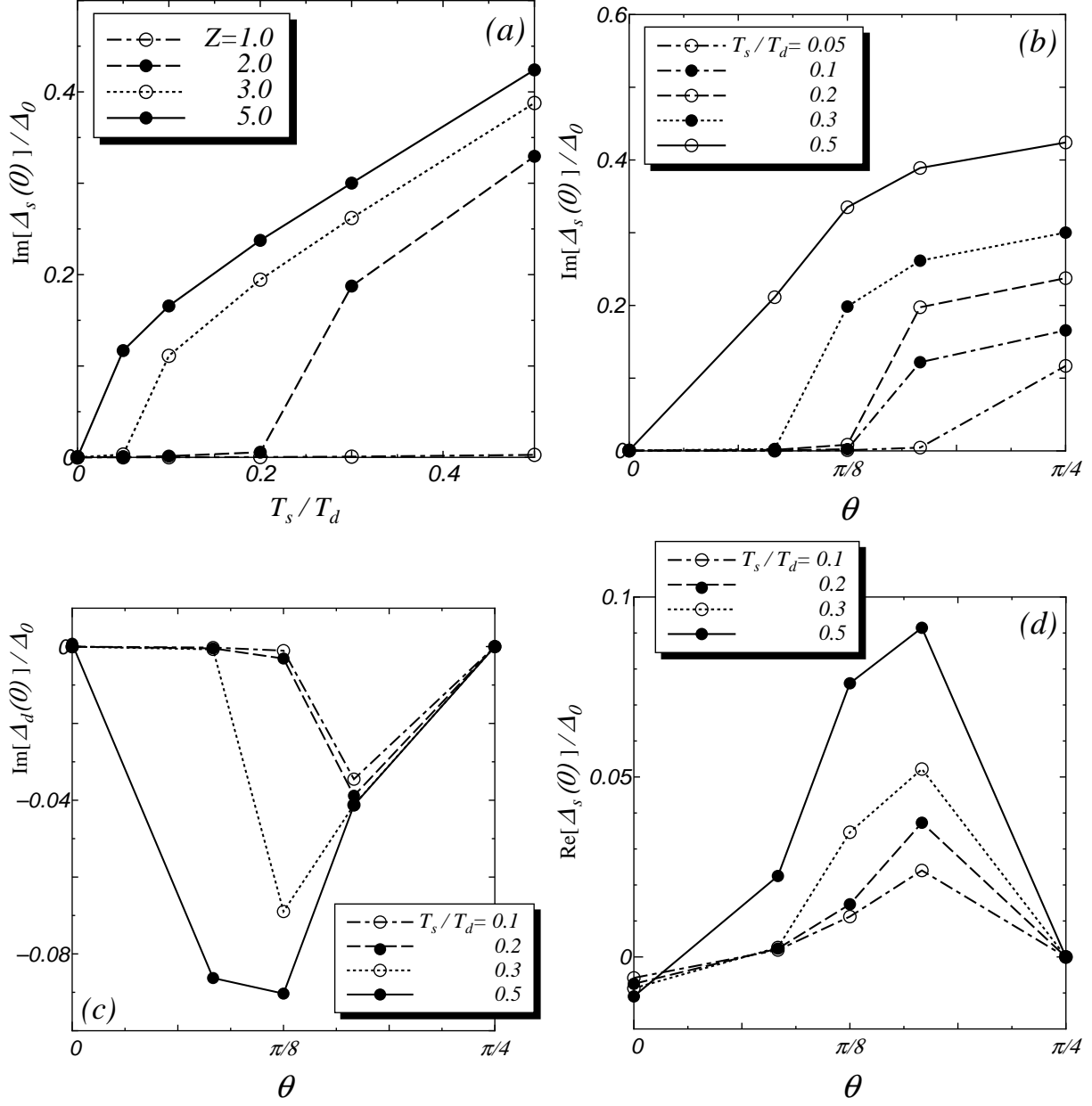


FIG. 3. Subdominant components of the pair potentials at the interface. $T = 0.05T_c$.

(a) $\theta = \pi/4$. $Z = 5.0$ for (b), (c), and (d).

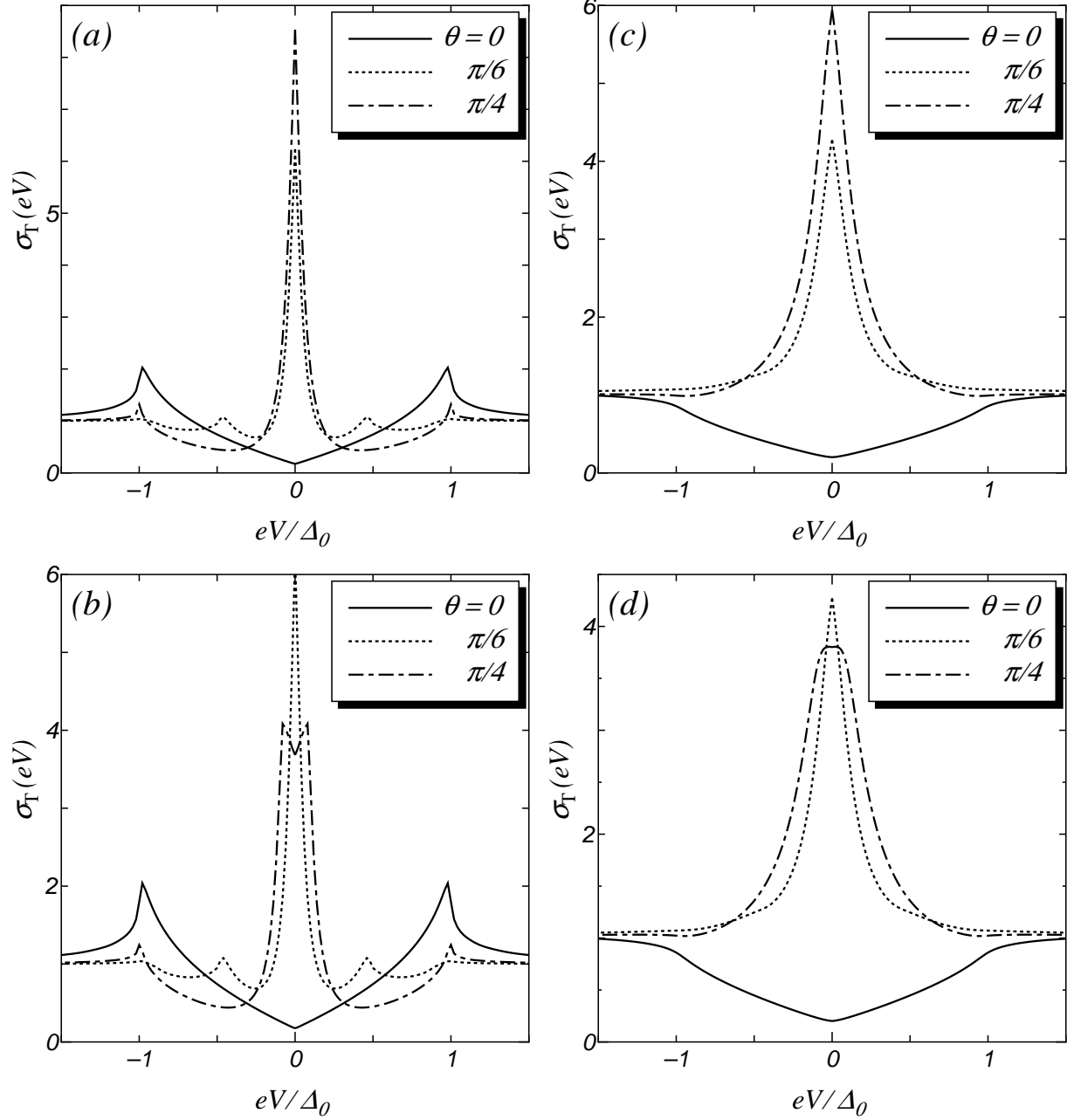


FIG. 4. The normalized tunneling conductance in the $d_{x^2-y^2}+is$ -wave state near the interface at $Z = 3.0$. $T_s/T_d = 0.05$ for (a) and (c). $T_s/T_d = 0.1$ for (b) and (d). $T = 0$ for (a) and (b). $T/T_c = 0.05$ for (c) and (d).

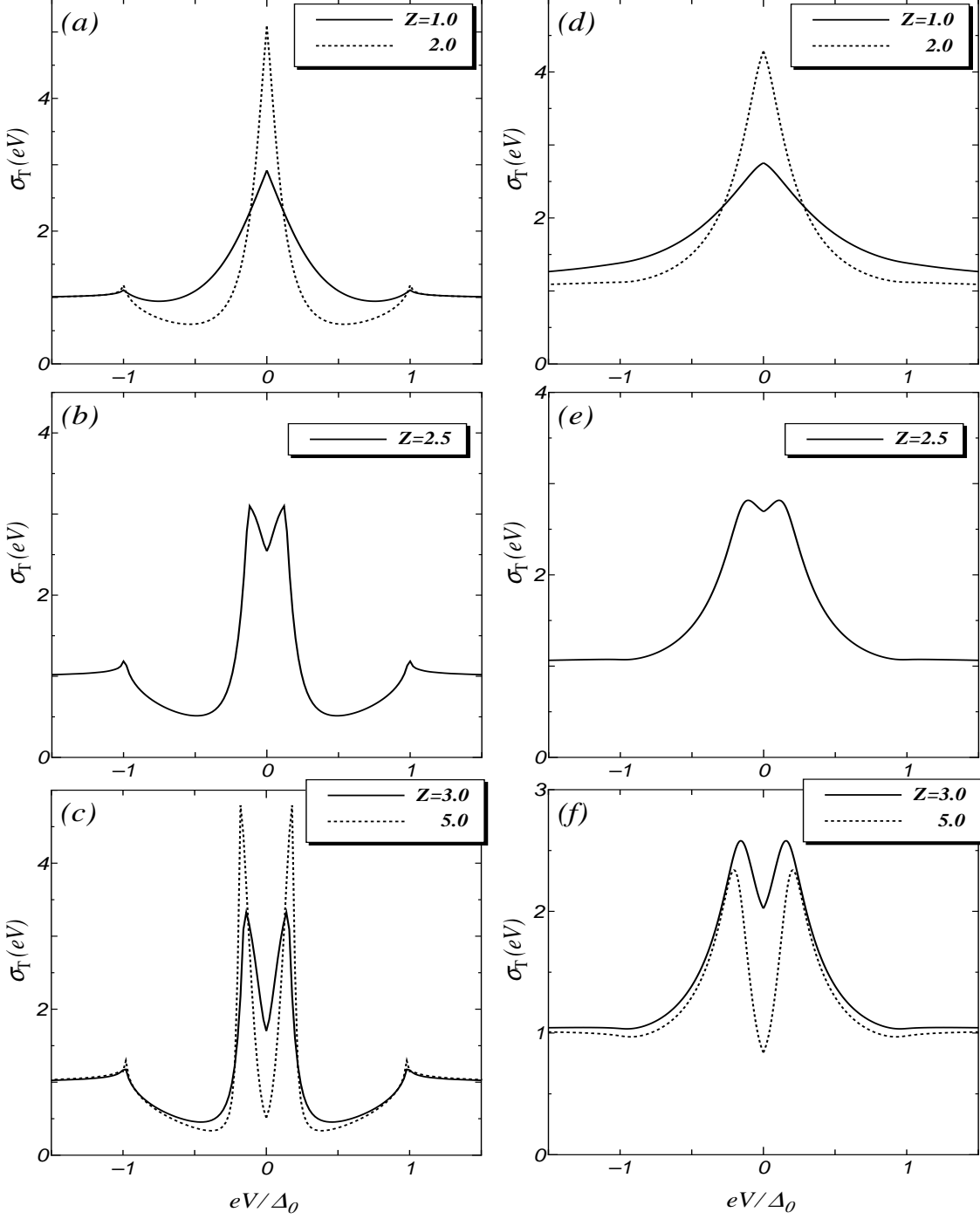


FIG. 5. Tunneling conductance for $d_{x^2-y^2}+is$ -wave state with $T_s/T_d = 0.2$ and $\theta = \pi/4$ for various Z ; (a) [(d)] low barrier ($Z = 1.0, 2.0$) (b) [(e)] middle barrier ($Z = 2.5$), and (c) [(f)] high barrier ($Z = 3.0, 5.0$). $T = 0$ for (a), (b), and (c). $T/T_c = 0.05$ for (d), (e), and (f).

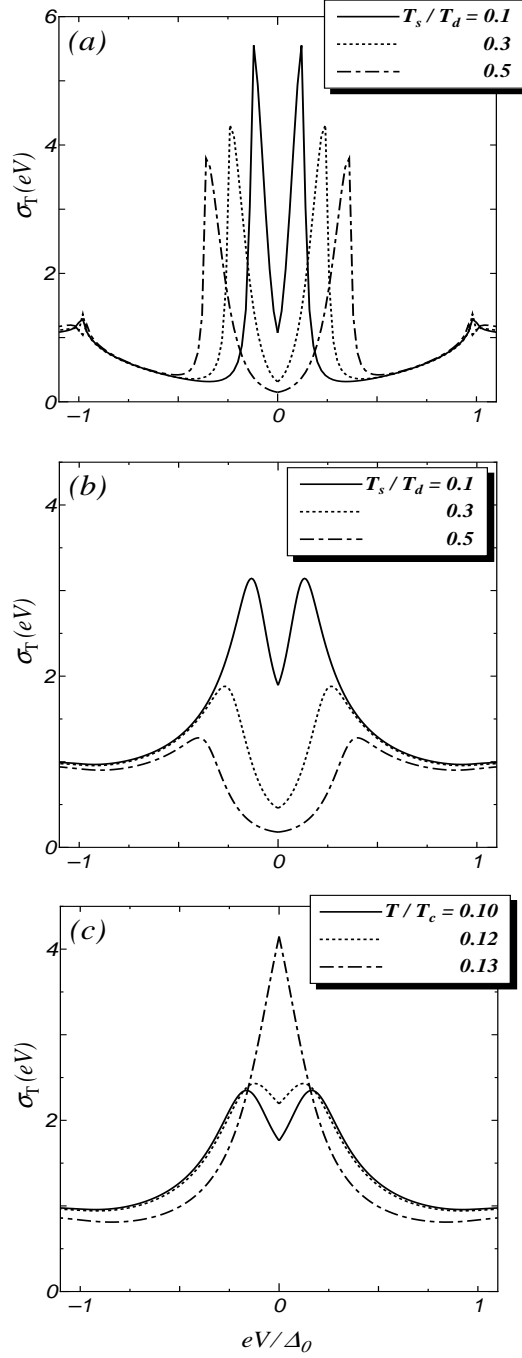


FIG. 6. Tunneling conductance for $d_{x^2-y^2}+is$ -wave state. $Z = 5$ and $\theta = \pi/4$. (a) $T = 0$, (b) $T = 0.05T_c$ for various magnitude of T_s . (c) various temperature with $T_s/T_d = 0.2$.

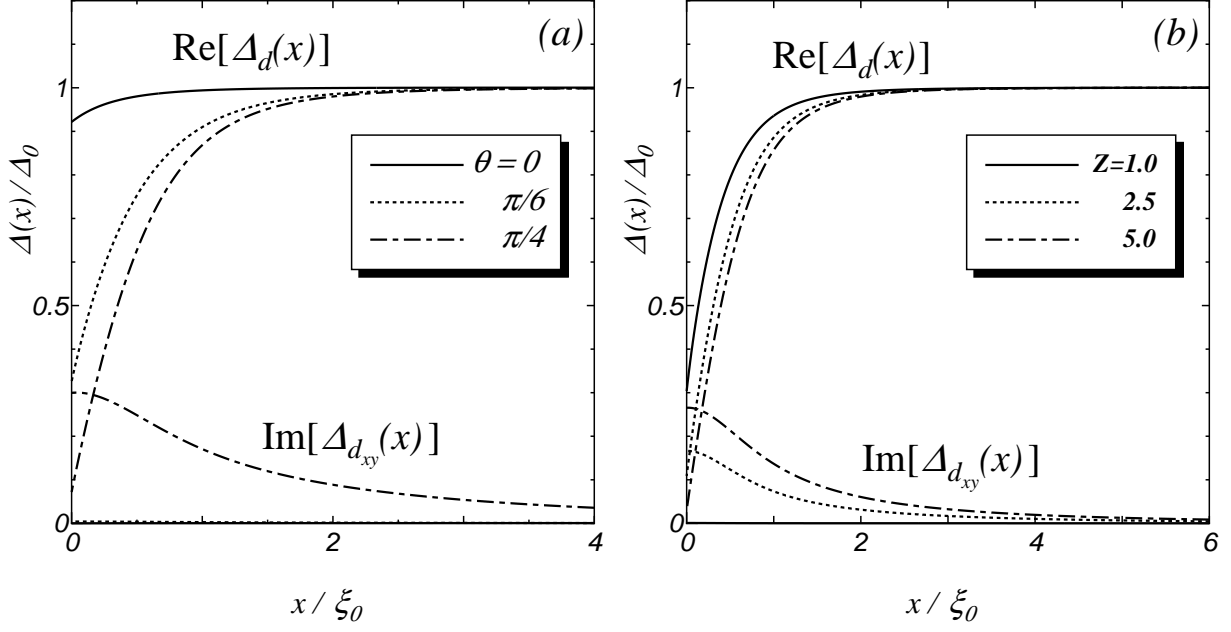


FIG. 7. Spatial dependences of the pair potential with $T_{d_{xy}}/T_d = 0.2$. $T = 0.05T_c$. (a) $Z = 3.0$ for various θ . (b) $\theta = 0$ for various Z .

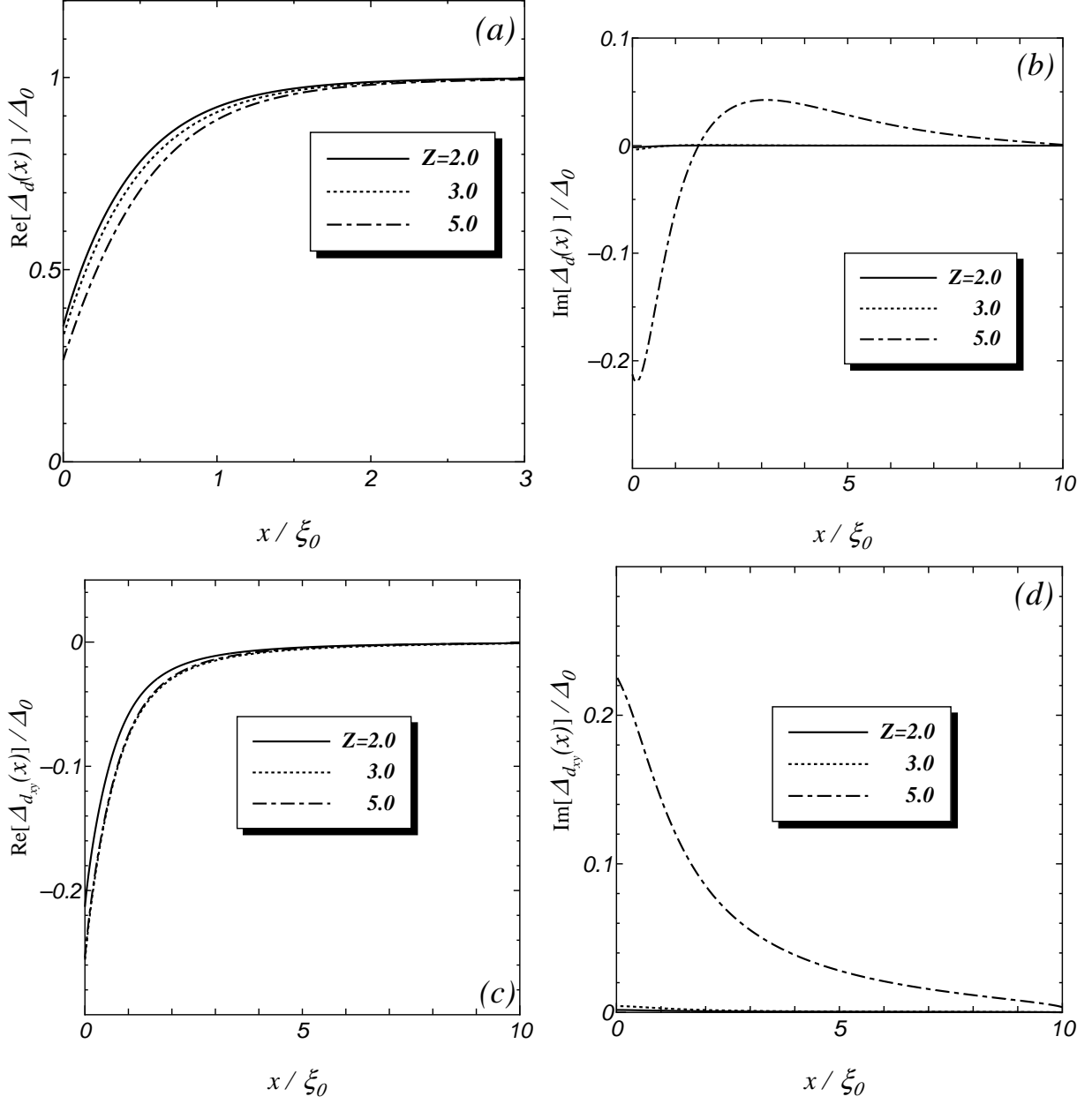


FIG. 8. Spatial dependence of the pair potentials near the interface with $\theta = \pi/6$ and $T_{d_{xy}}/T_d = 0.3$; (a) real part of $\Delta_d(x)$, (b) imaginary part of $\Delta_d(x)$, (c) real part of $\Delta_{d_{xy}}(x)$, and (d) imaginary part of $\Delta_{d_{xy}}(x)$. $T = 0.02T_c$.

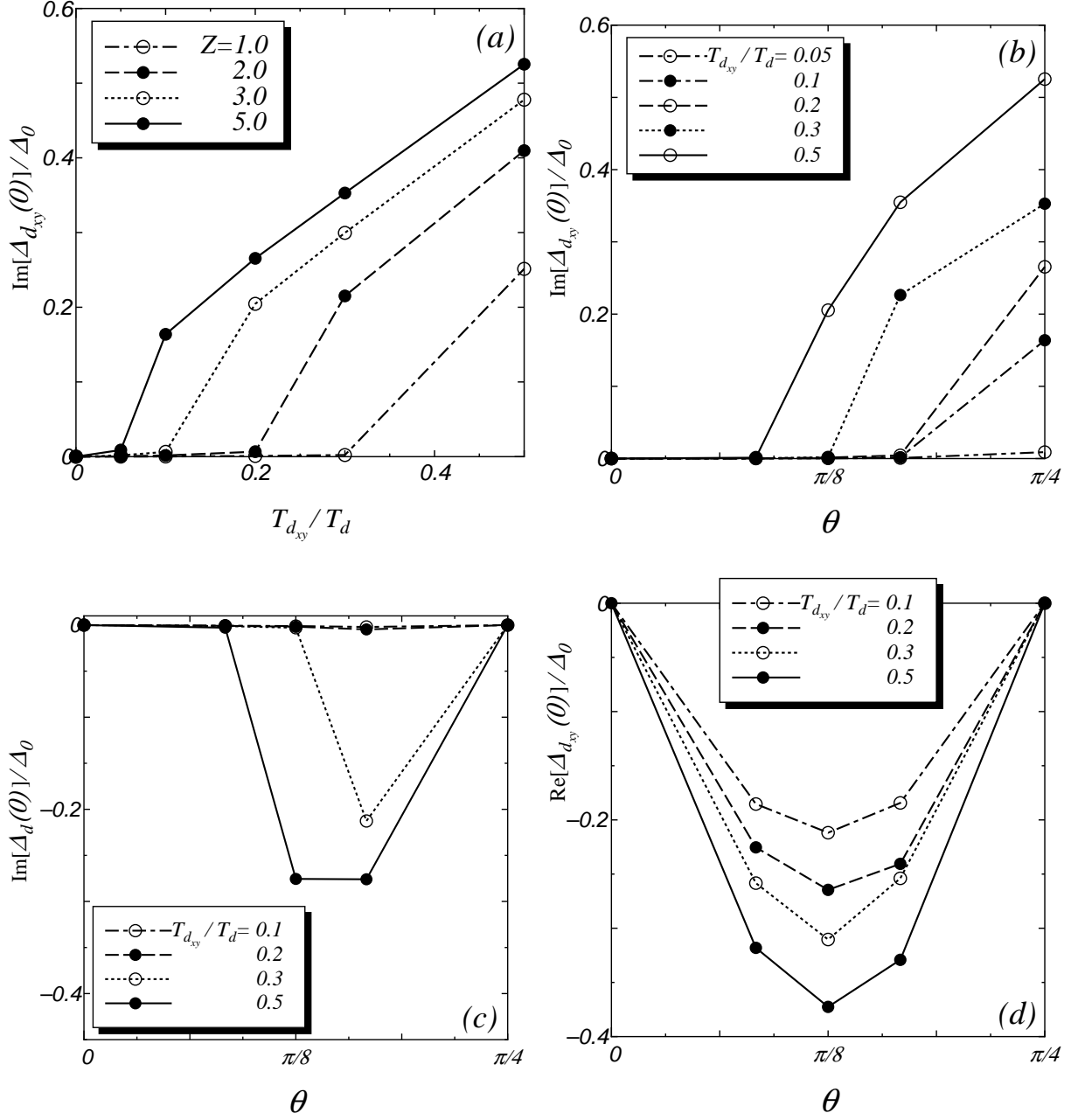


FIG. 9. Subdominant components of the pair potentials at the interface. $T = 0.05T_c$. (a) $\theta = \pi/4$. $Z = 5.0$ for (b), (c), and (d).

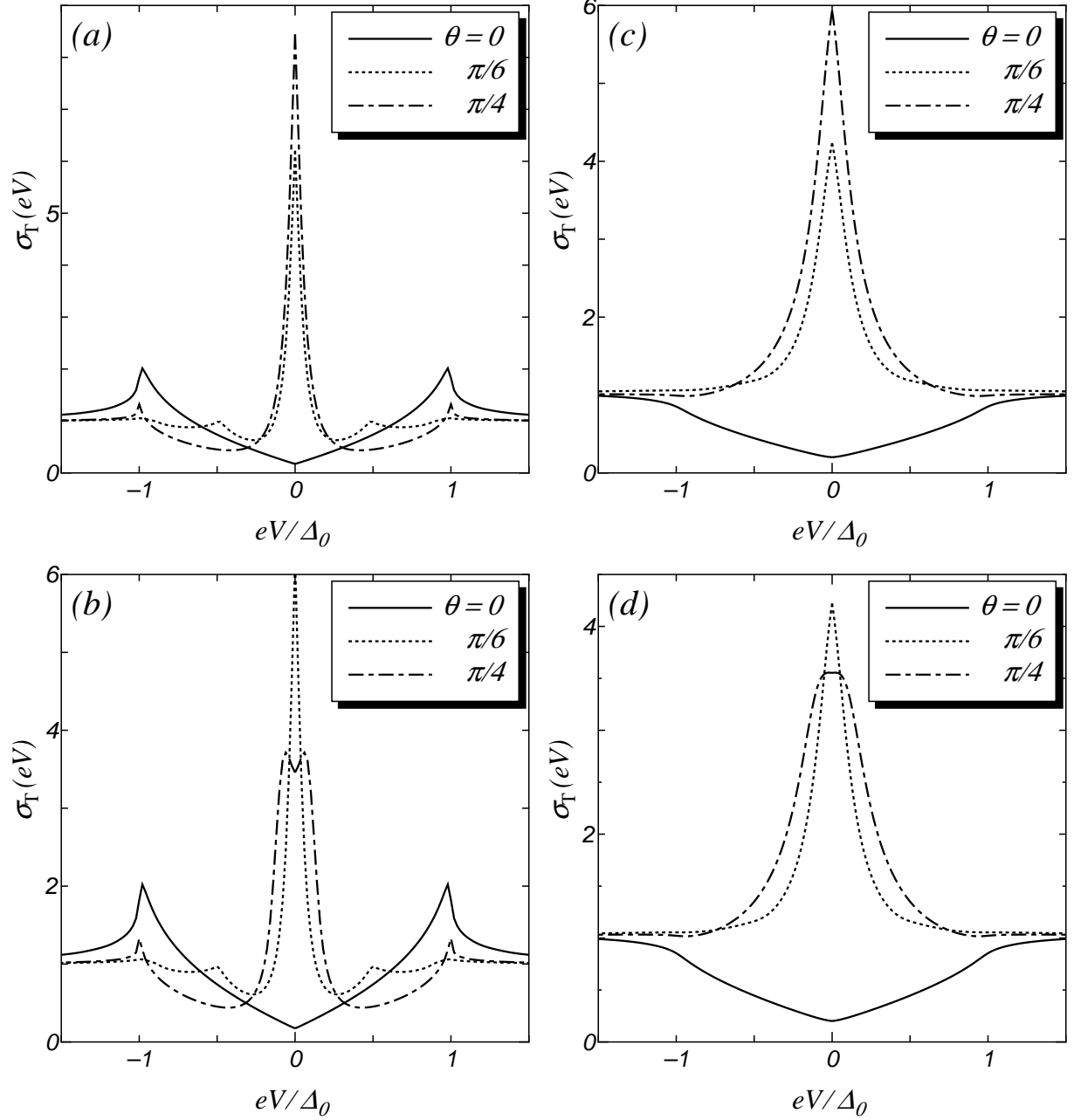


FIG. 10. The normalized tunneling conductance for $d_{x^2-y^2} + i d_{xy}$ -wave state with $Z = 3.0$. (a) $T_{d_{xy}}/T_d = 0.1$ and $T = 0.0$. (b) $T_{d_{xy}}/T_d = 0.2$ and $T = 0.0$. (c) $T_{d_{xy}}/T_d = 0.1$ and $T = 0.05T_c$. (d) $T_{d_{xy}}/T_d = 0.2$ and $T = 0.05T_c$.

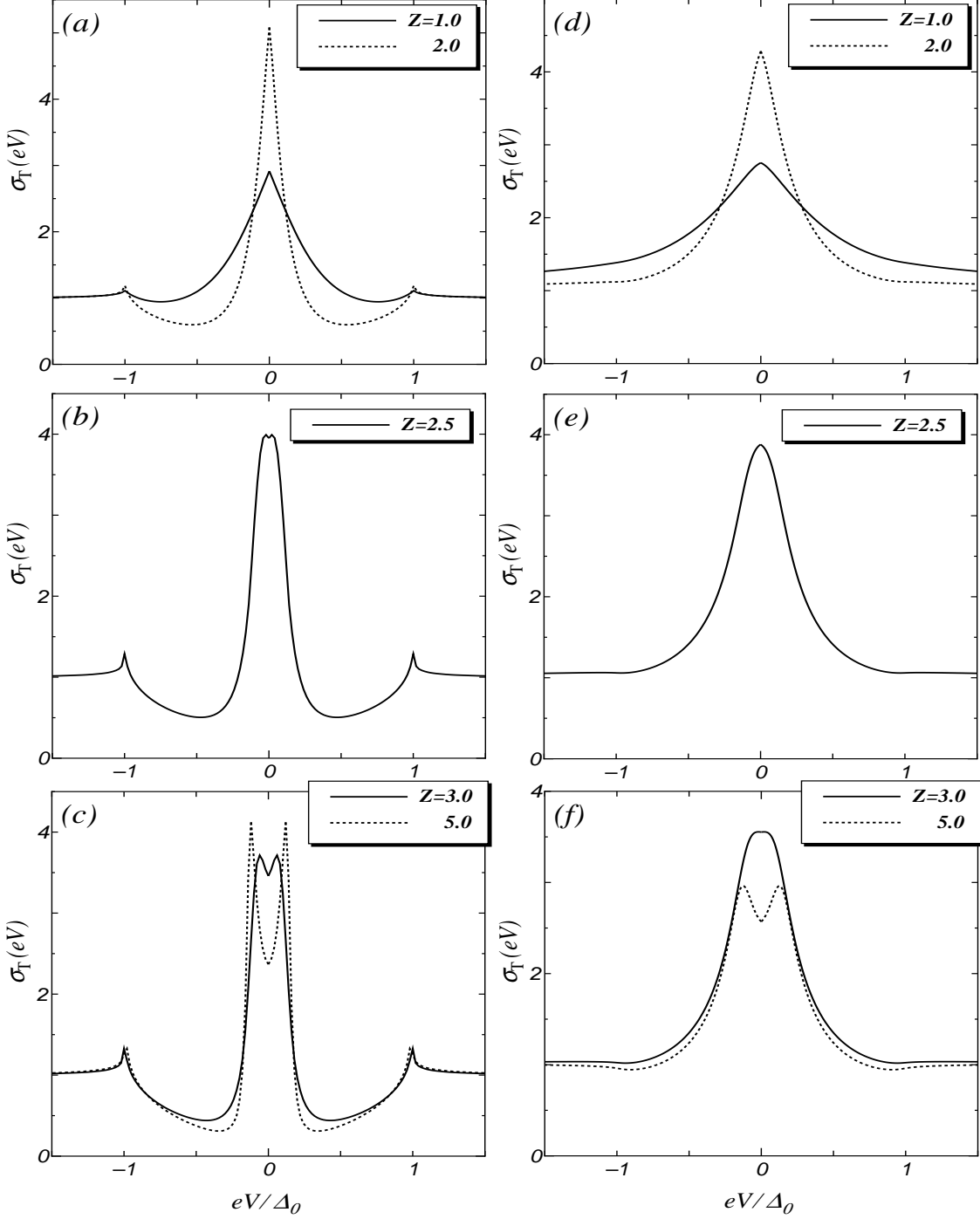


FIG. 11. Tunneling conductance for $d_{x^2-y^2}+id_{xy}$ -wave state with $\theta = \pi/4$ and $T_{d_{xy}}/T_d = 0.2$ for various Z . (a) [(d)] low barrier ($Z = 1.0, 2.0$) (b) [(e)] middle barrier ($Z = 2.5$), and (c) [(f)] high barrier ($Z = 3.0, 5.0$). $T = 0$ for (a), (b), and (c). $T = 0.05T_c$ for (d), (e), and (f).

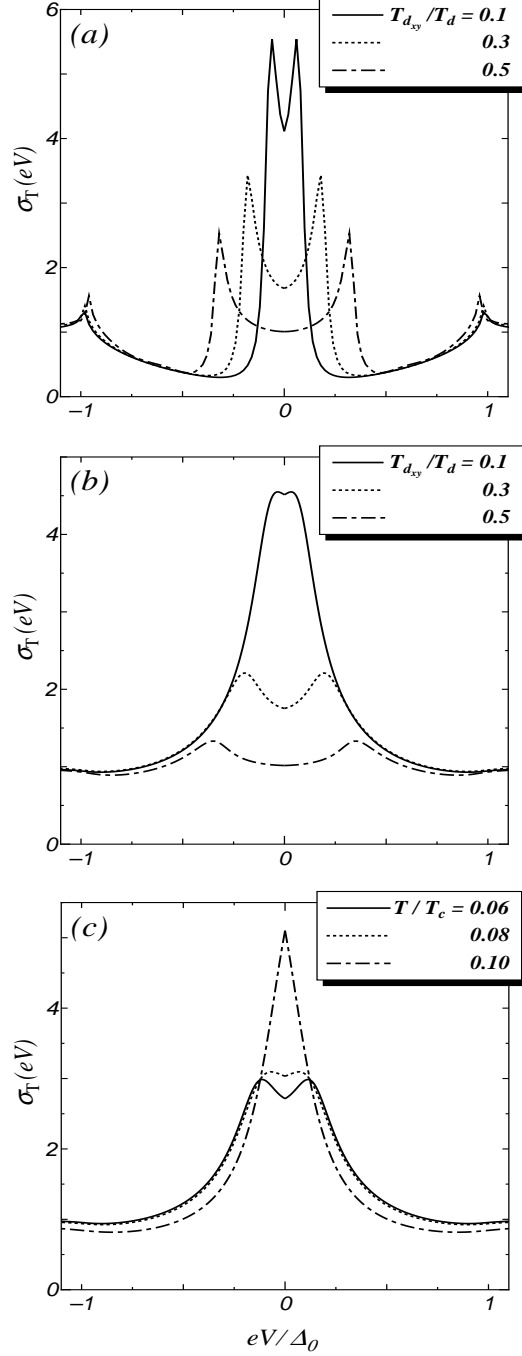


FIG. 12. Tunneling conductance for $d_{x^2-y^2} + id_{xy}$ -wave state with $\theta = \pi/4$ and $Z = 5$. (a) $T = 0$, (b) $T = 0.05T_c$ for various magnitude of T_s . (c) various temperature with $T_s/T_d = 0.2$.